Multiple Instabilities in the Entropy Layer of a Hypersonic Blunt Cone

Lachlan Whyborn, Rowan Gollan, Peter Jacobs

Centre for Hypersonics, School of Mechanical and Mining Engineering, University of Queensland

uqlwhybo@uq.edu.au

January 24, 2023

Overview of Boundary Layer Transition

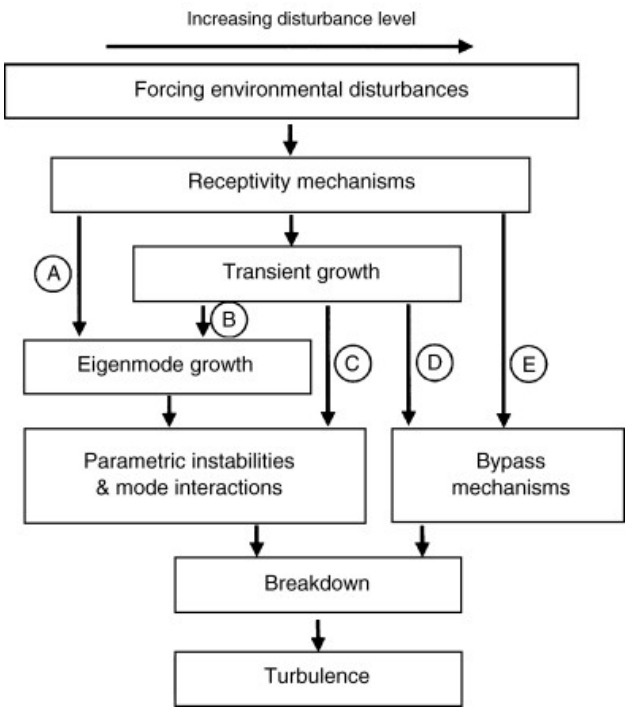

Reshotko's paths to transition. Increasing environmental forcing from left to right.

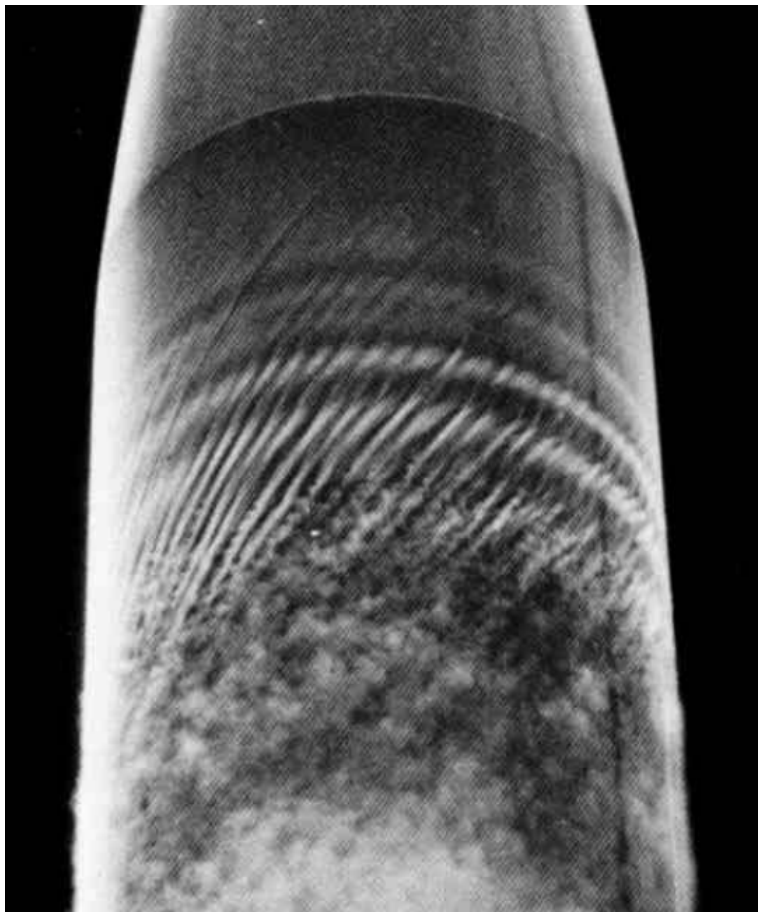

Smoke visualisation of Tollmien-Schlichting and crossflow instabilities interacting and leading to transition.

Overview of Boundary Layer Transition

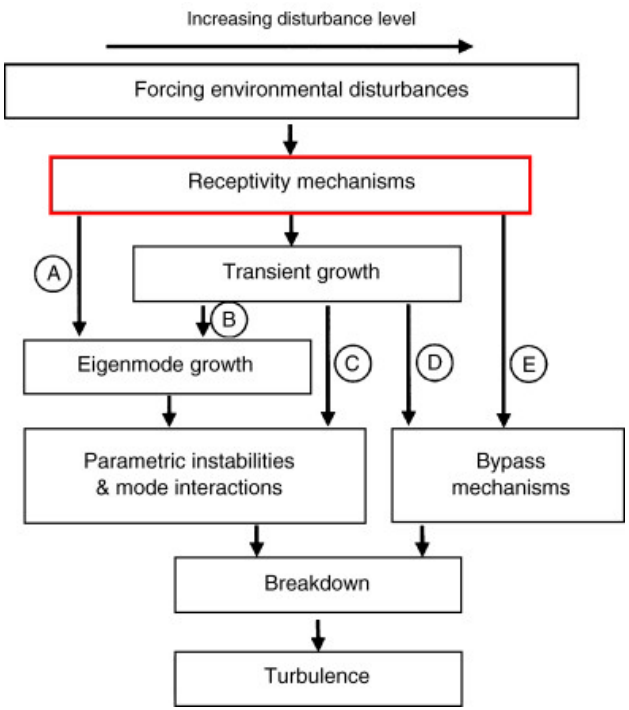

Reshotko's paths to transition. Increasing environmental forcing from left to right.

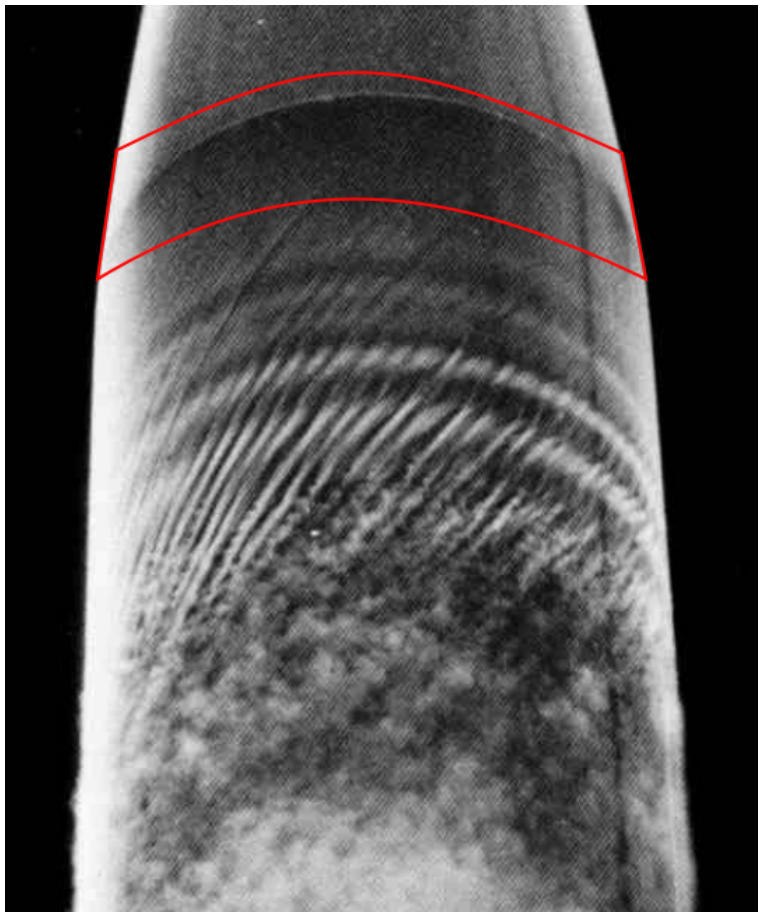

Smoke visualisation of Tollmien-Schlichting and crossflow instabilities interacting and leading to transition.

Overview of Boundary Layer Transition

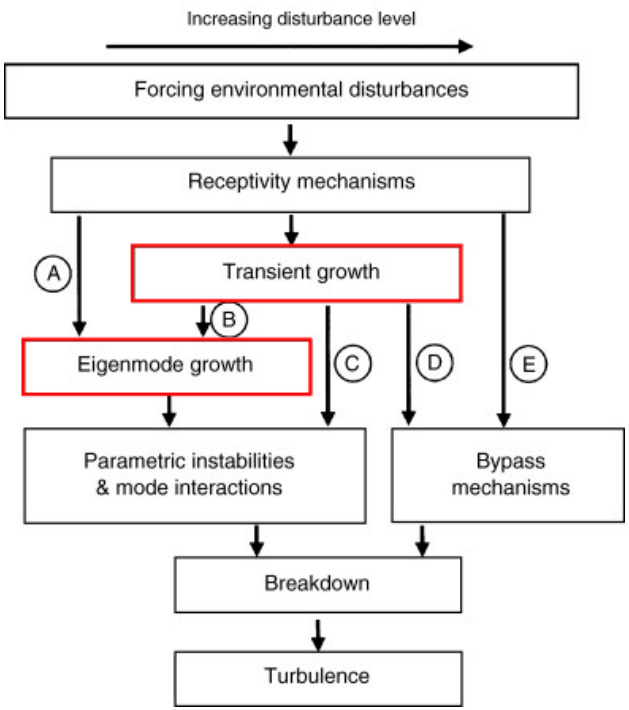

Reshotko's paths to transition. Increasing environmental forcing from left to right.

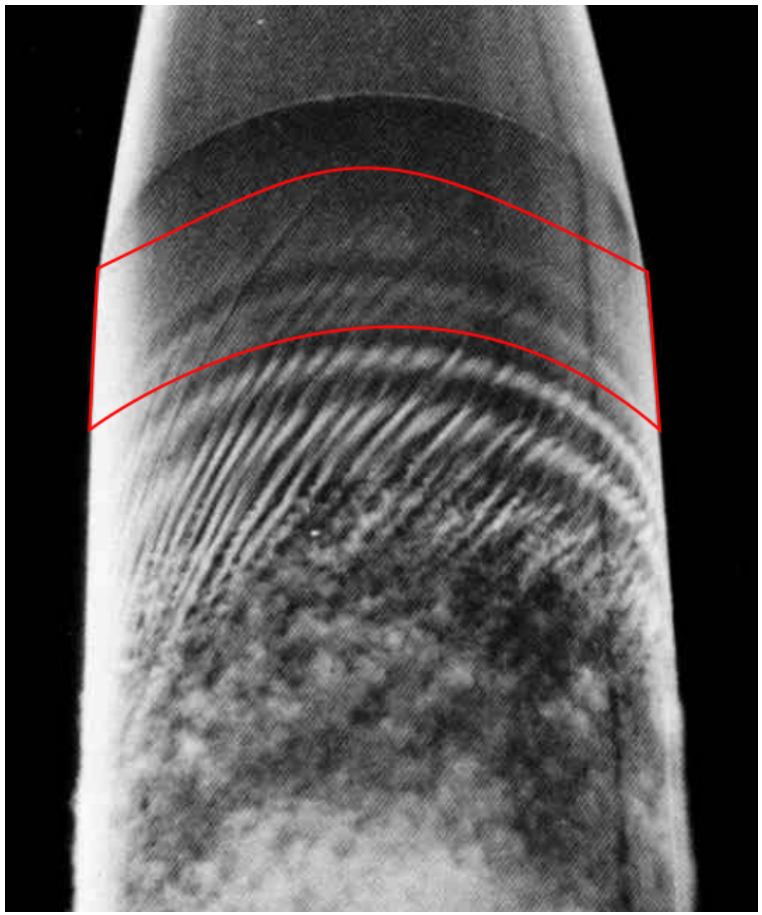

Smoke visualisation of Tollmien-Schlichting and crossflow instabilities interacting and leading to transition.

Overview of Boundary Layer Transition

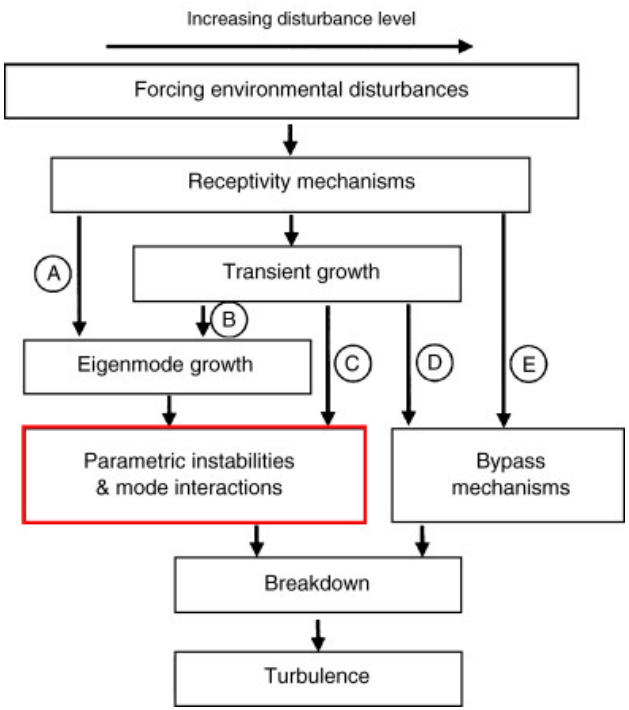

Reshotko's paths to transition. Increasing environmental forcing from left to right.

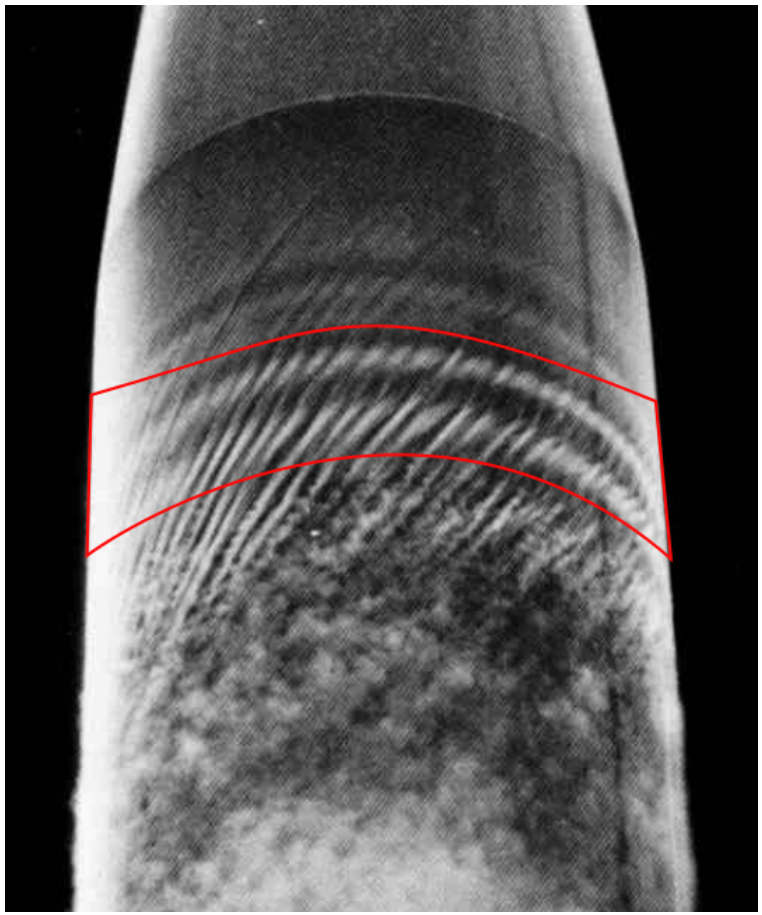

Smoke visualisation of Tollmien-Schlichting and crossflow instabilities interacting and leading to transition.

Overview of Boundary Layer Transition

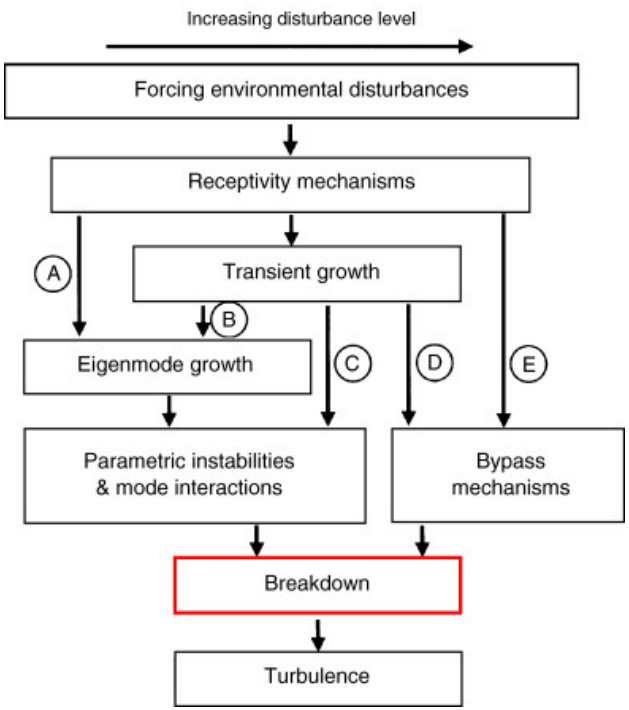

Reshotko's paths to transition. Increasing environmental forcing from left to right.

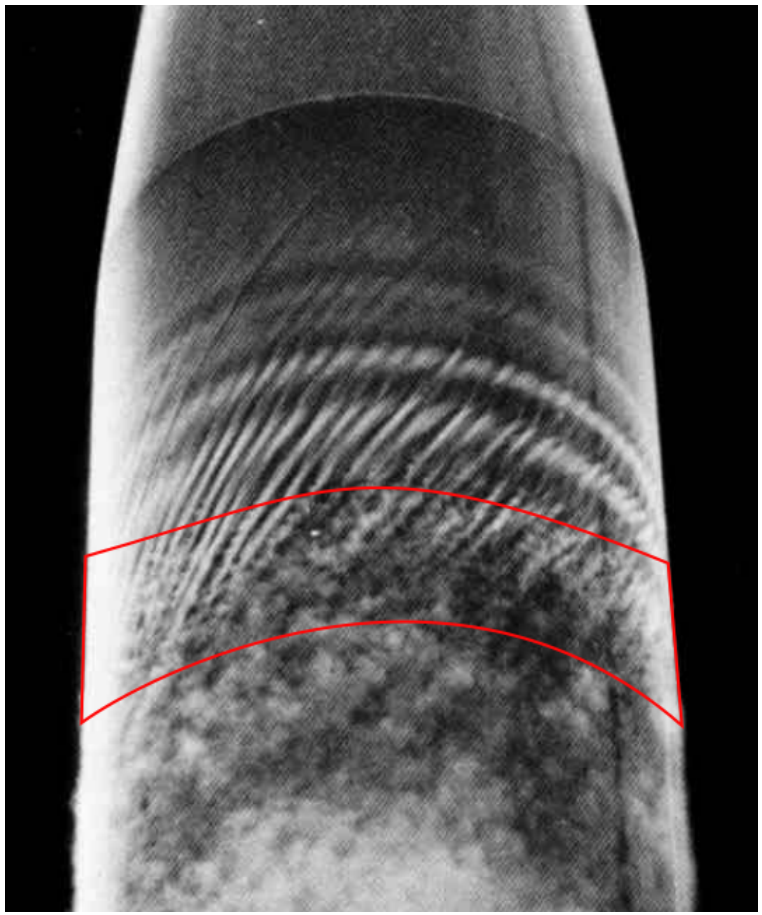

Smoke visualisation of Tollmien-Schlichting and crossflow instabilities interacting and leading to transition.

Overview of Boundary Layer Transition

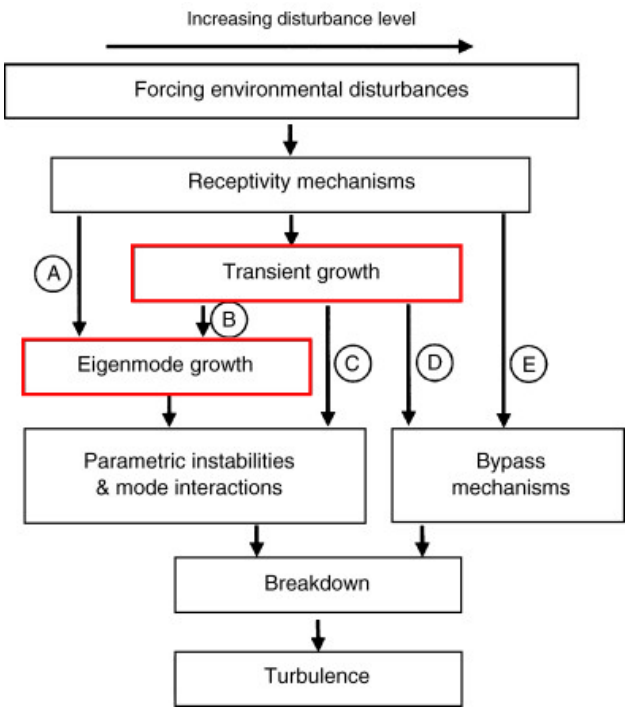

Reshotko's paths to transition. Increasing environmental forcing from left to right.

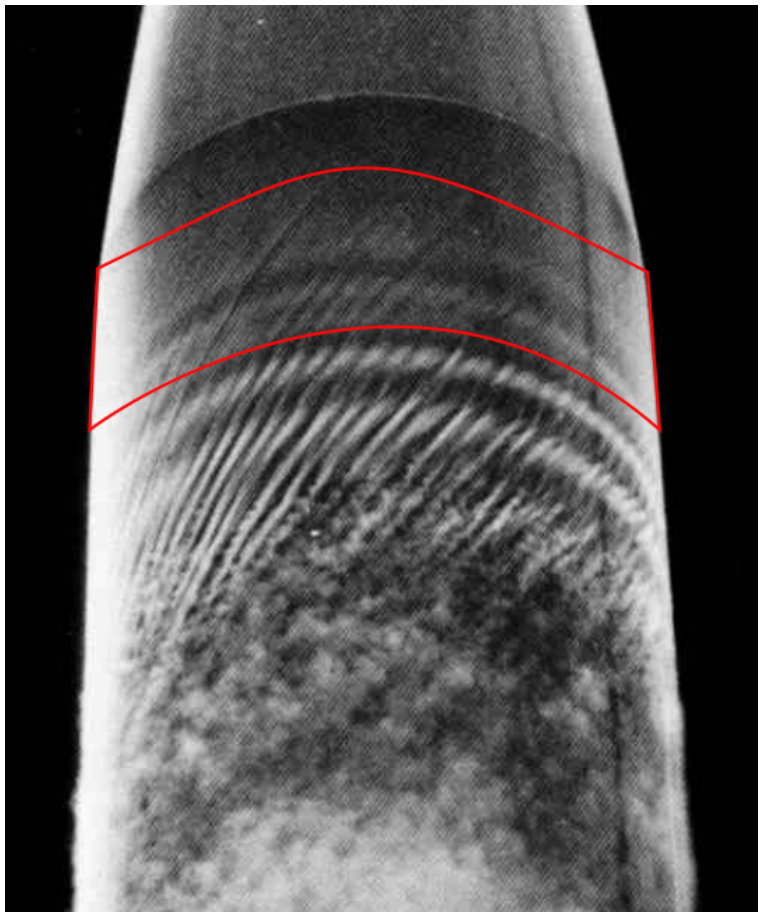

Smoke visualisation of Tollmien-Schlichting and crossflow instabilities interacting and leading to transition.

Blunting Effects on Boundary Layer Transition

Leading edge bluntness initially delays boundary layer transition through supression of the second mode, then the trend reverses.

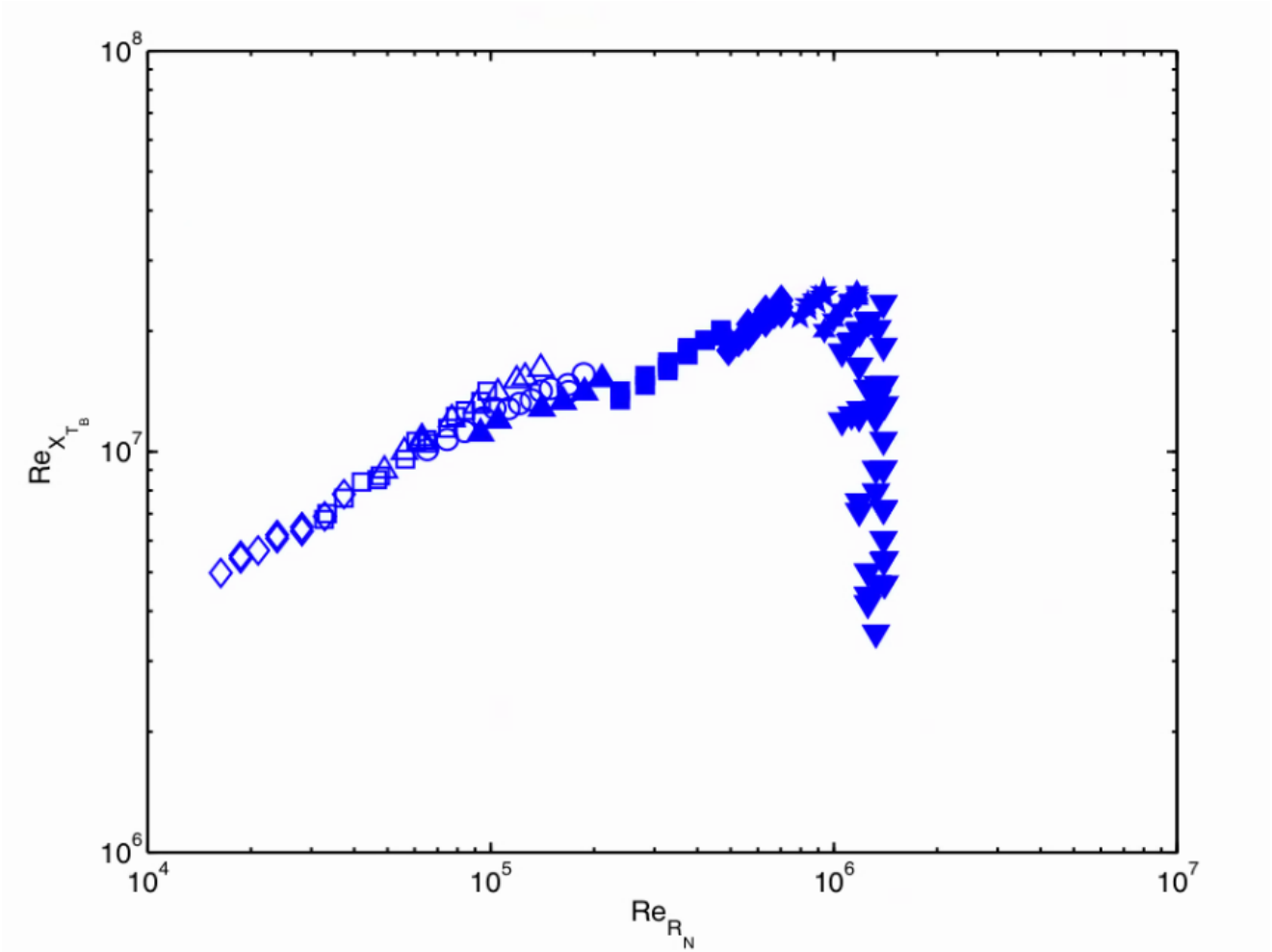

Effect of nose bluntness on transition, from R. Kimmel and J. Jewell.

Blunting Effects on Boundary Layer Transition

Leading edge bluntness initially delays boundary layer transition through supression of the second mode, then the trend reverses.

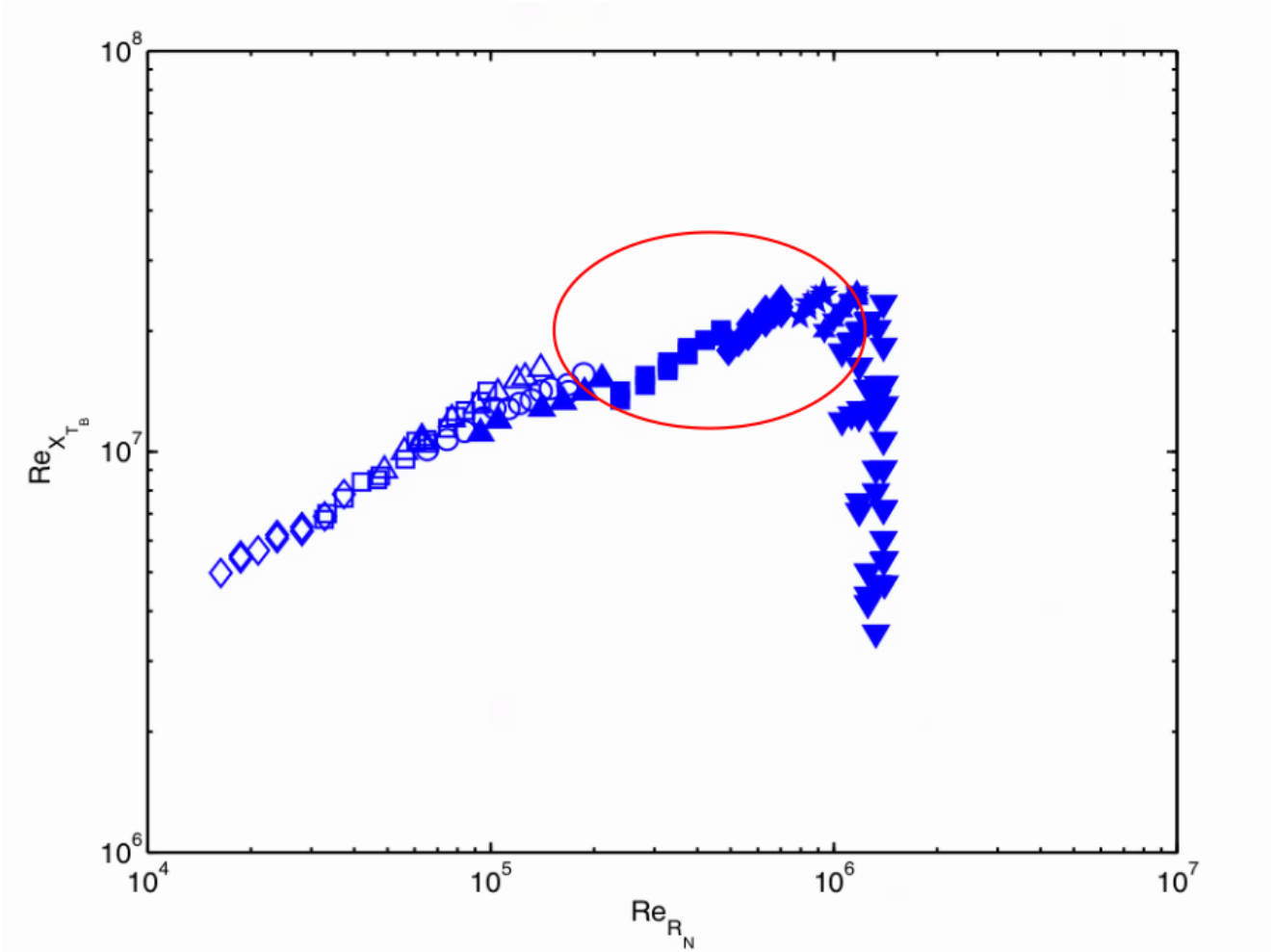

Effect of nose bluntness on transition, from R. Kimmel and J. Jewell.

The Geometry and Flow Conditions

Chosen to match the geometry and conditions of Stetson et al.

$$M_\infty = 7.99$$
$$p_\infty = 413.68\text{Pa}$$
$$T_\infty = 54.47\text{K}$$
$$Re_\infty = 8.202 \times 10^6$$

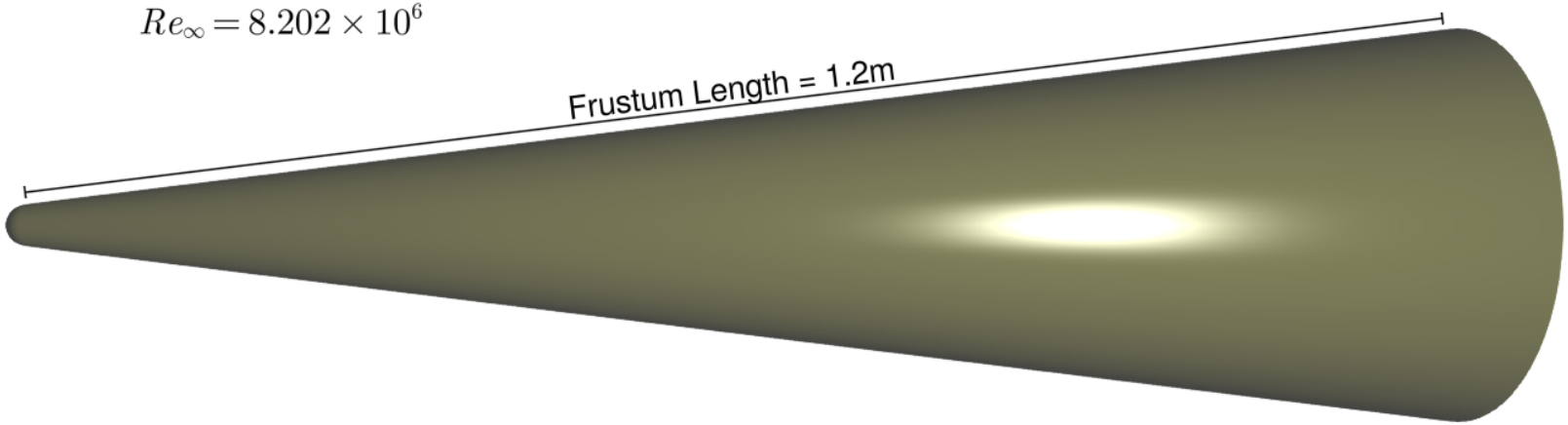

$$\text{Nose Radius} = 17.78\text{mm}$$
$$\text{Half Angle} = 7°$$

The Inflection Point

A generalized inflection point exists in the entropy layer for most conditions.

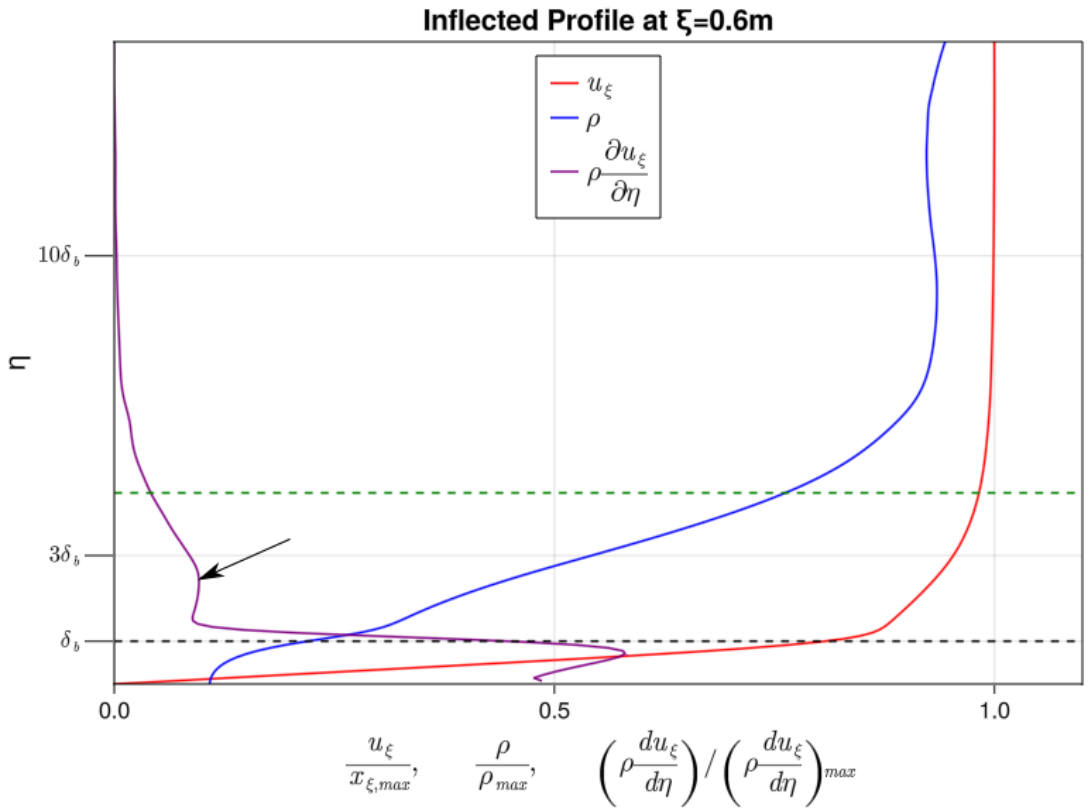

Wallnormal profiles at $\xi = 0.6m$ for the flow of interest.

The Mean Base Flow

$M_\infty = 7.99$

$p_\infty = 413.68\text{Pa}$

$T_\infty = 54.47\text{K}$

$Re_\infty = 8.202 \times 10^6$

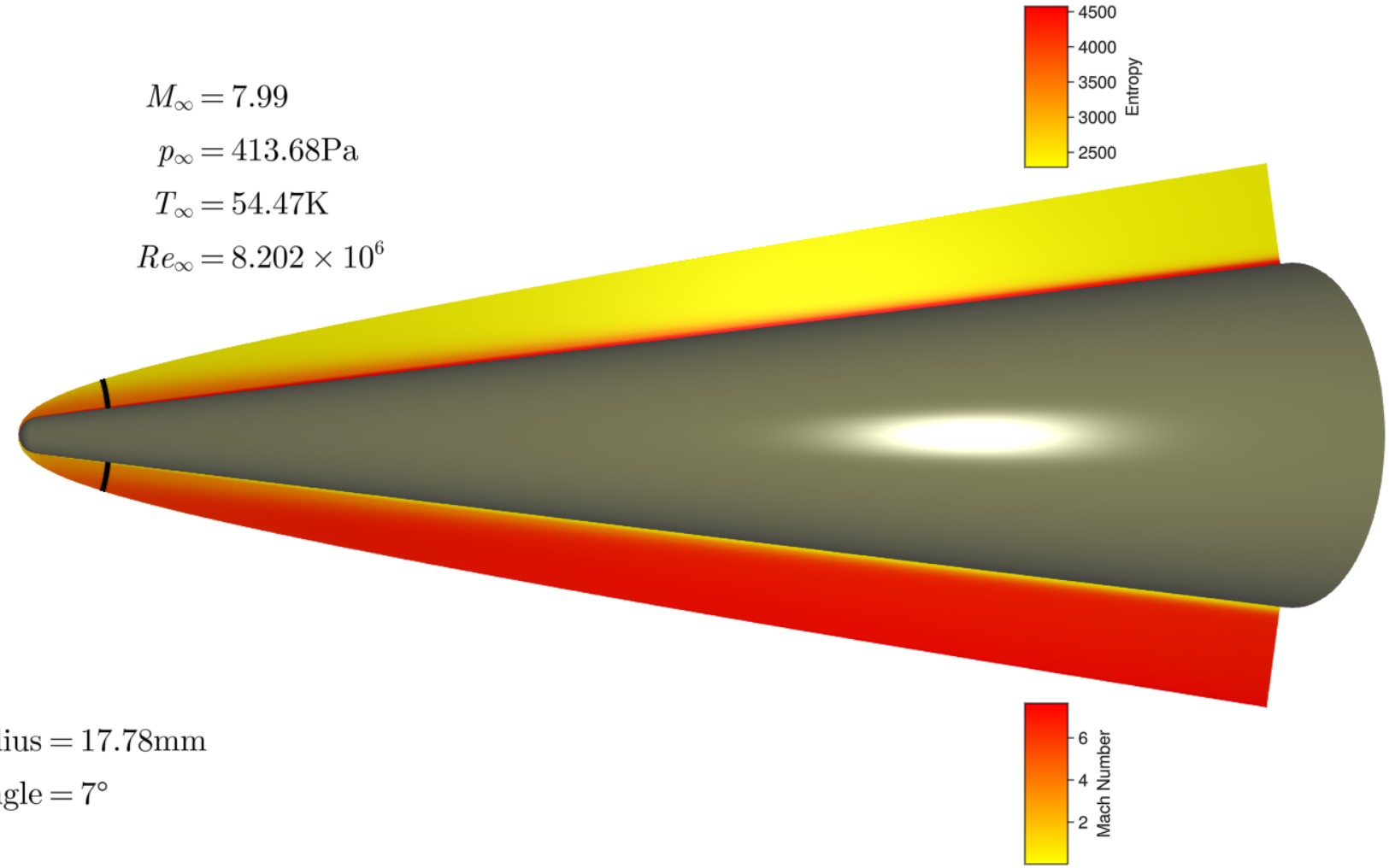

$\text{Nose Radius} = 17.78\text{mm}$

$\text{Half Angle} = 7°$

Inflow Disturbance Function

Impose a gaussian shaped disturbance function on the inflow plane. Series of frequencies from 0 to 150kHz.

$$p'_\infty = \sum_{n=1}^{60} A \sin(2\pi F_n t + k_{x,n} x + k_{y,n} y + R) \qquad \rho'_\infty = p'_\infty / \overline{a_\infty}^2 \qquad u'_{i,\infty} = p'_\infty$$

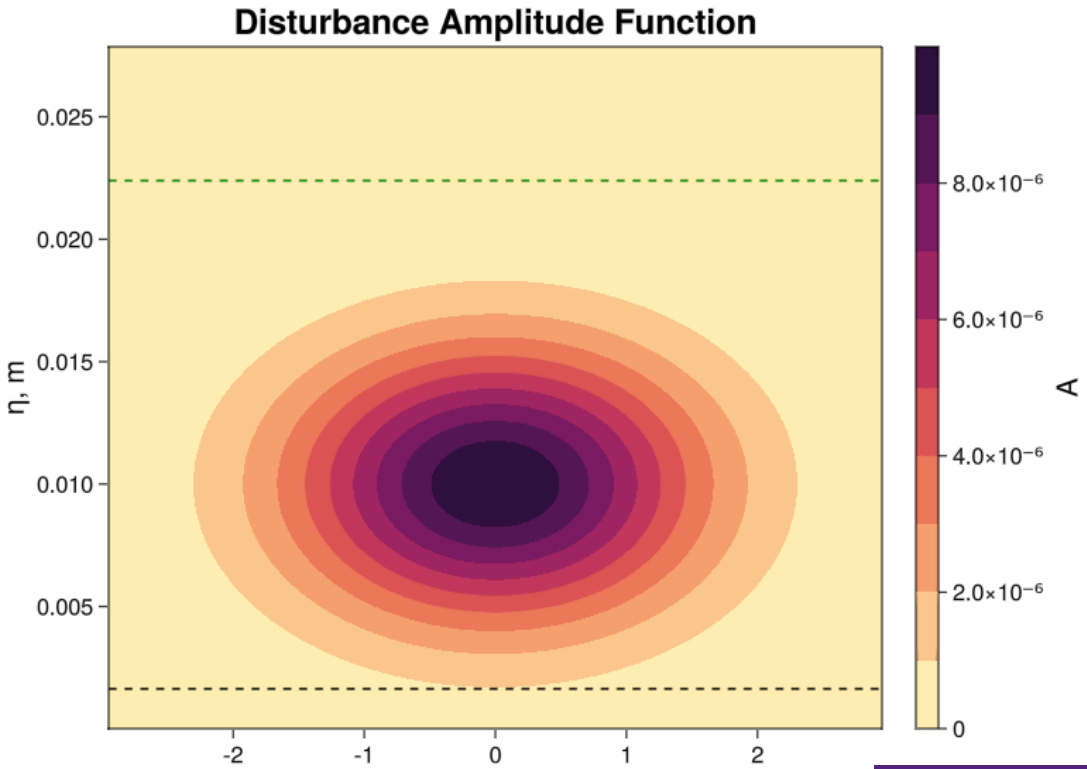

An Instantaneous Snapshot

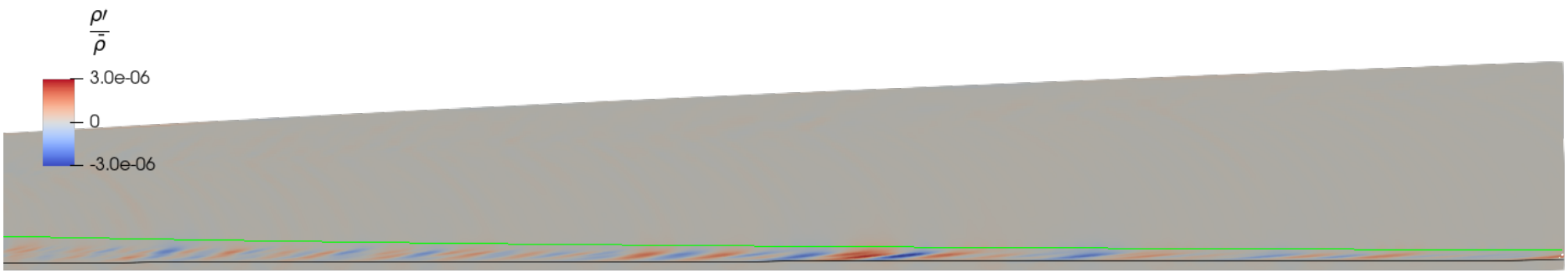

Instantaneous snapshot of the density fluctuations.

Comparison to Experimental Schlieren

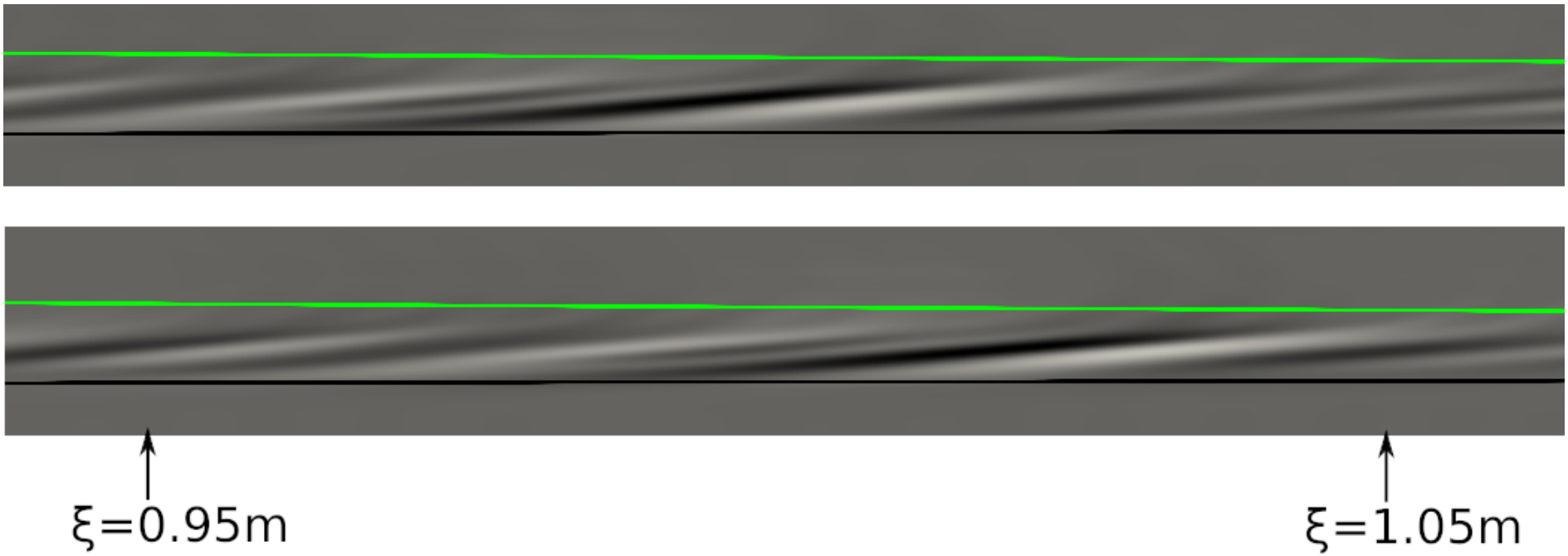

Numerical schlieren separated by 25μs. Propagation speed approximately 1.2 times the boundary layer edge velocity.

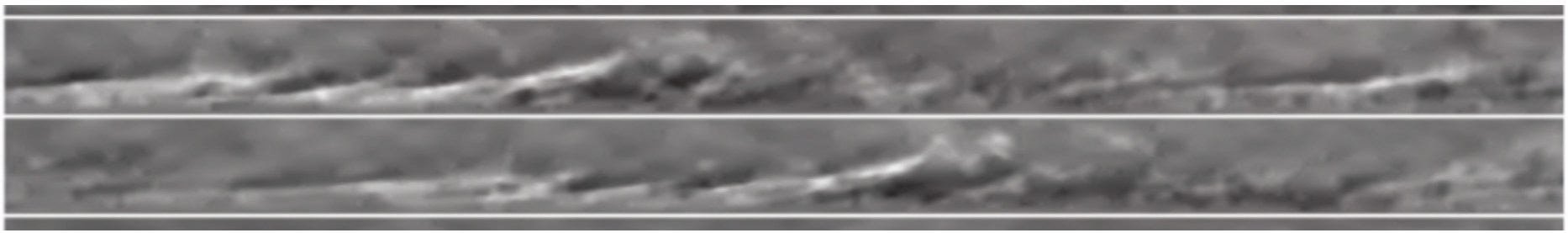

Schlieren images from Kennedy et al.. Propagation speed approximately 1.03 times the boundary layer edge velocity.

Comparison to Experimental Schlieren

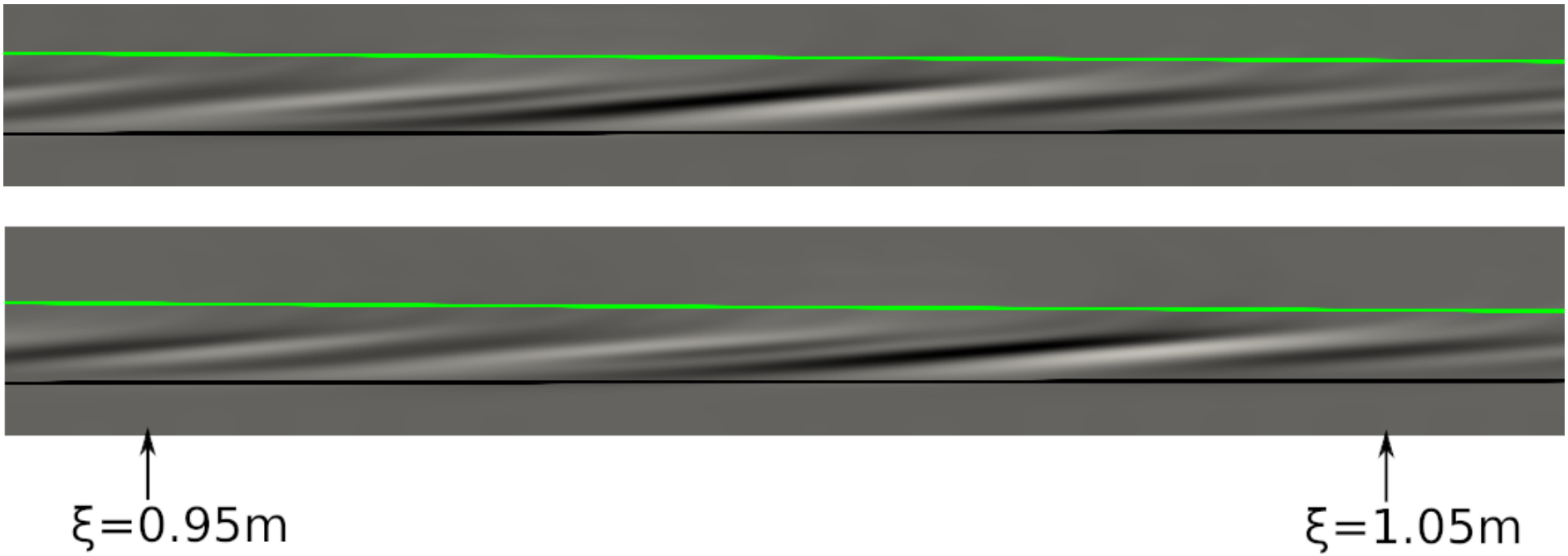

Numerical schlieren separated by 25μs. Propagation speed approximately 1.2 times the boundary layer edge velocity.

Schlieren images from Kennedy et al.. Propagation speed approximately 1.03 times the boundary layer edge velocity.

Fourier Space

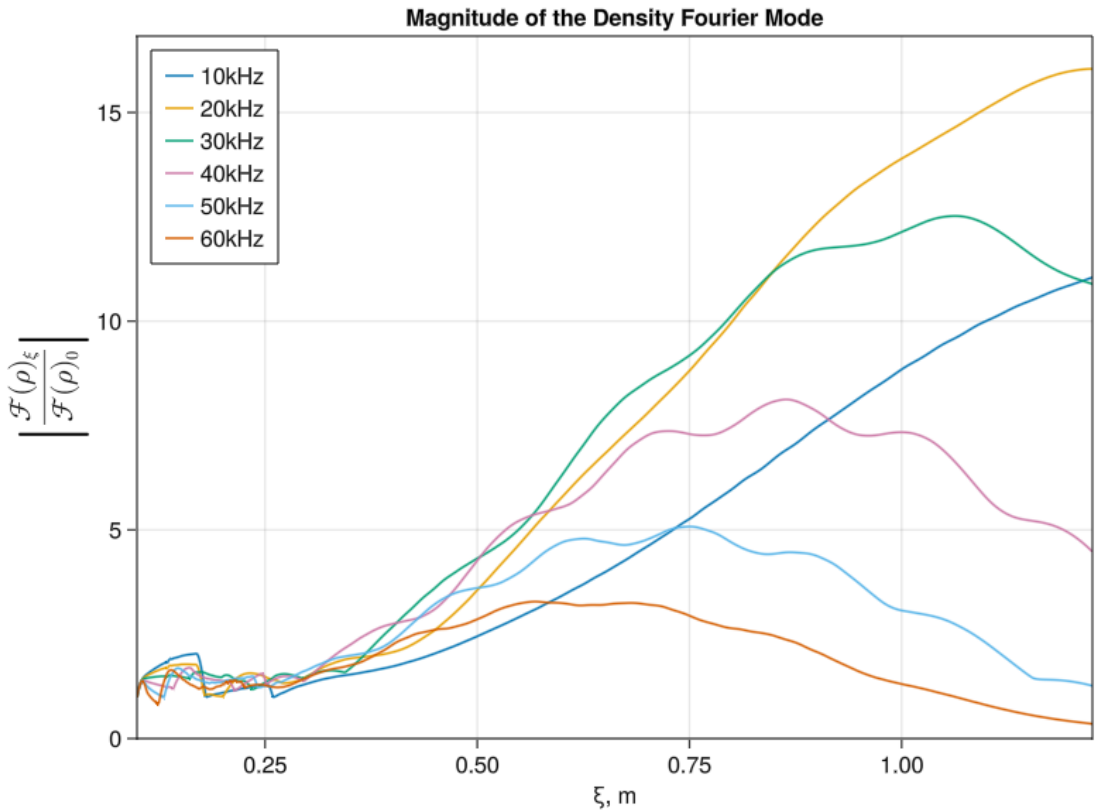

Spatial evolution of low frequency density fluctuations in the entropy layer.

Matches with typical transient growth behaviour- amplitude trend is $\xi \exp^{-\alpha\xi}$.

Shape of Density Fluctuations

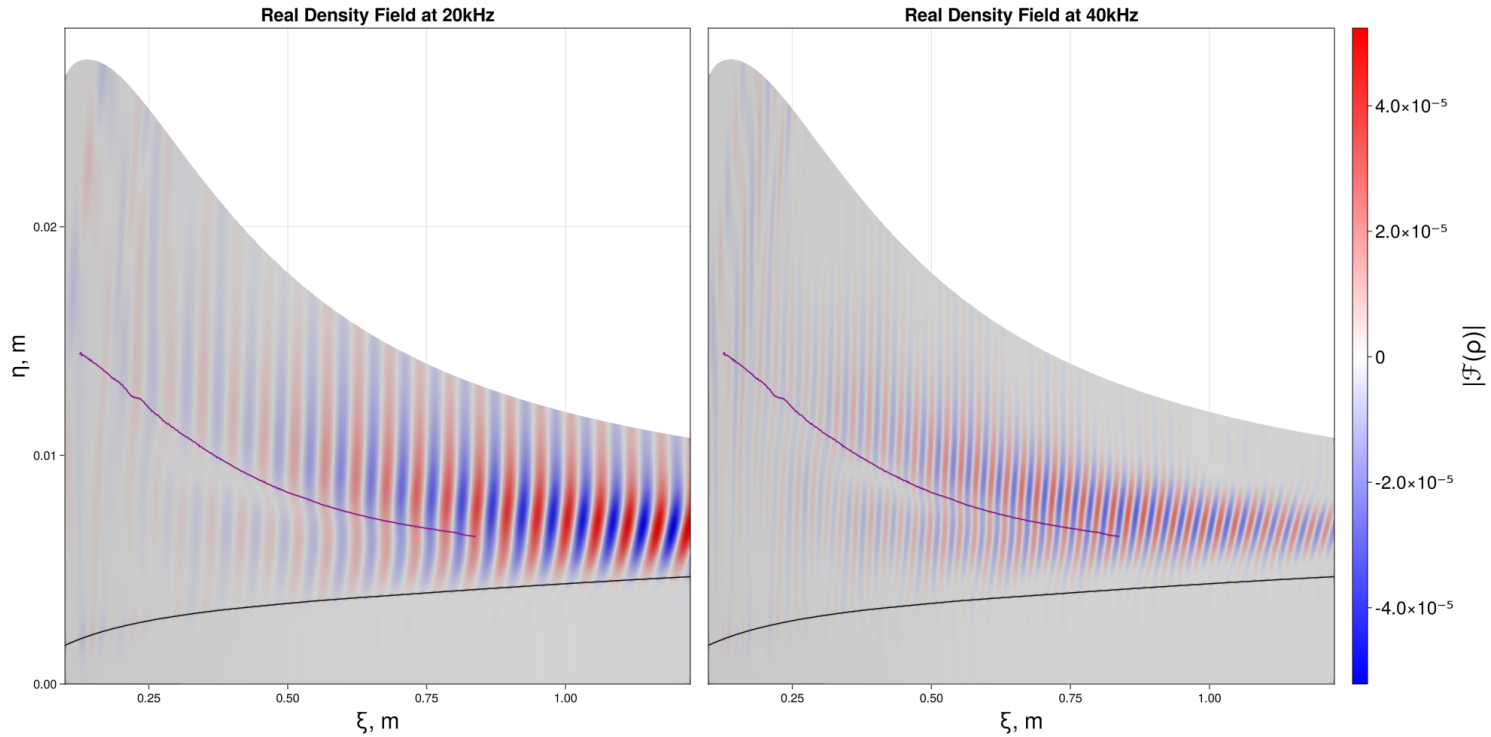

Real part of the 20kHz and 40kHz Fourier modes, showing the shape of the density fluctuations in the entropy layer.

Calculating the Group Velocity

Group velocity is expected to be same as the propagation speed of the density structures.

$$v_{phase} = \frac{\partial \omega}{\partial k} \qquad (1)$$

Group velocity is calculated to be 1125.8m/s, compared to 1150m/s from structure tracking.

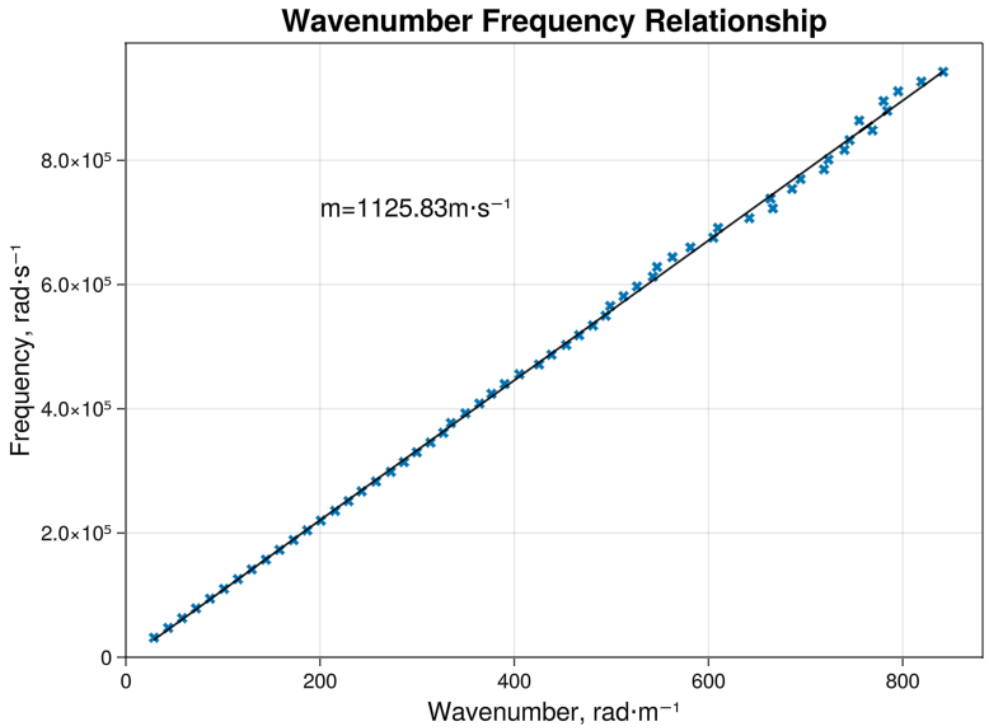

Relationship between wavenumber and frequency used to calculate the group velocity.

3D Simulation

Fluctuation amplitude much greater in 3D.

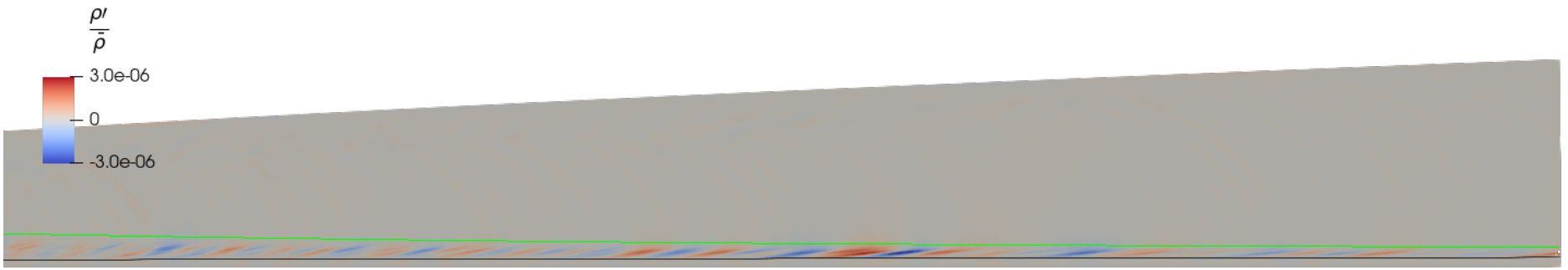

Density fluctuations in an axisymmetric domain.

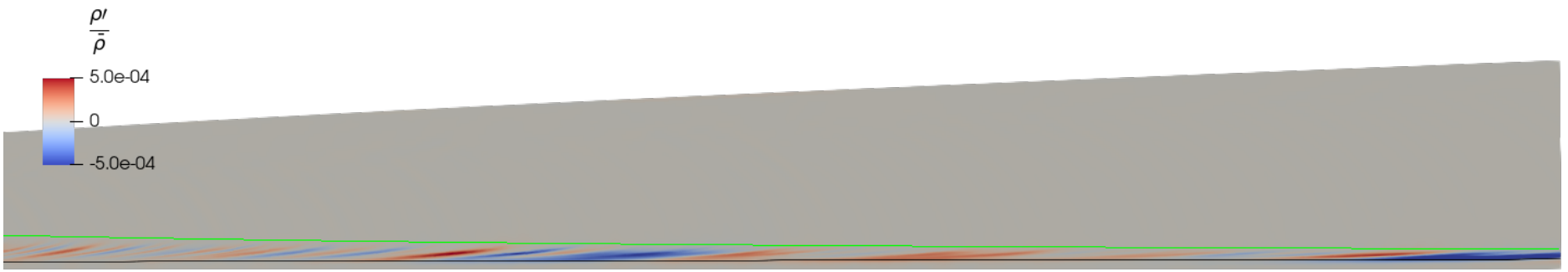

Density fluctuations in a 3D domain.

Amplitude of Density Disturbances

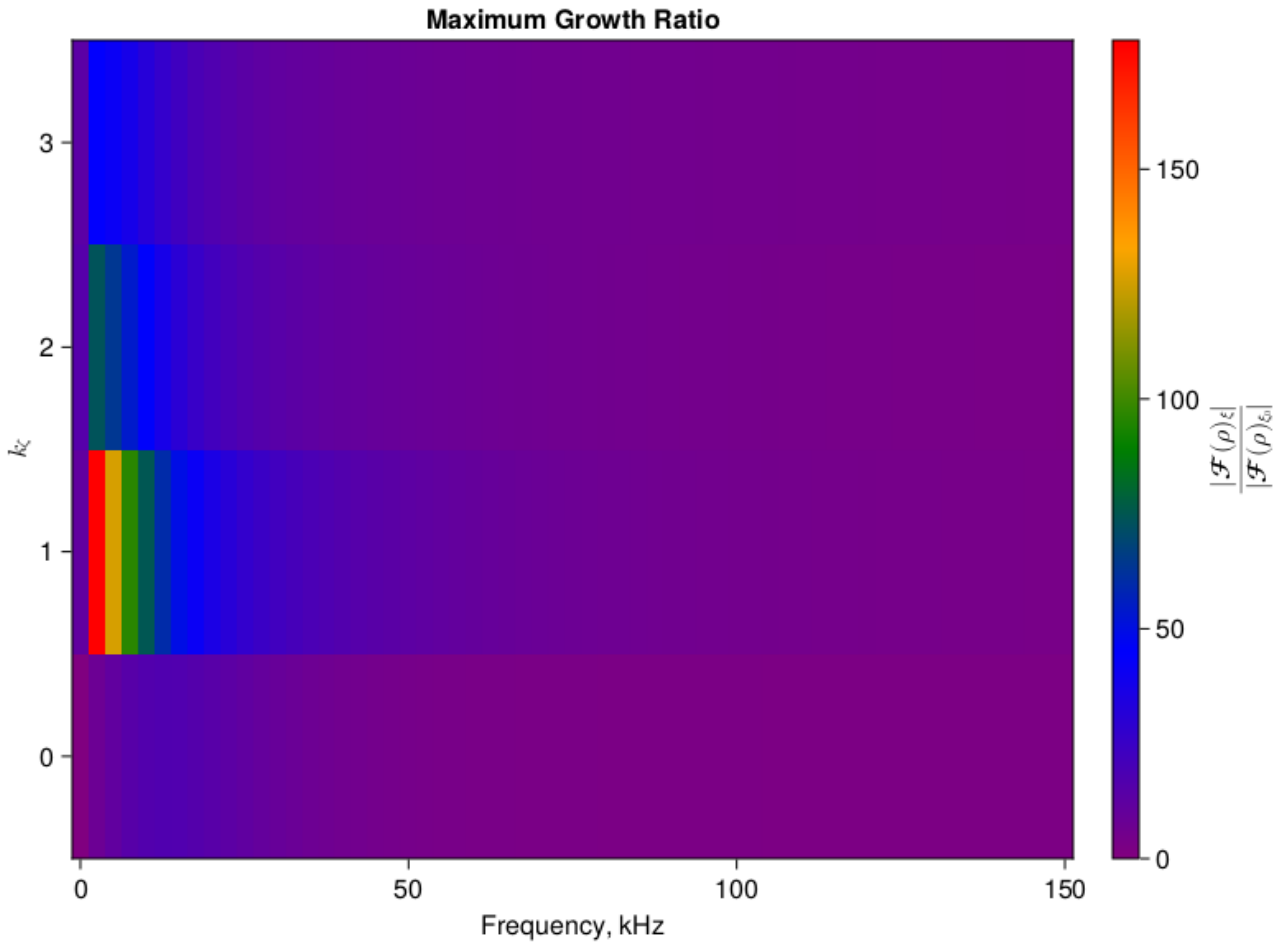

Peak growth ratio for each frequency and select spanwise wavenumbers.

Evolution of Density Disturbances

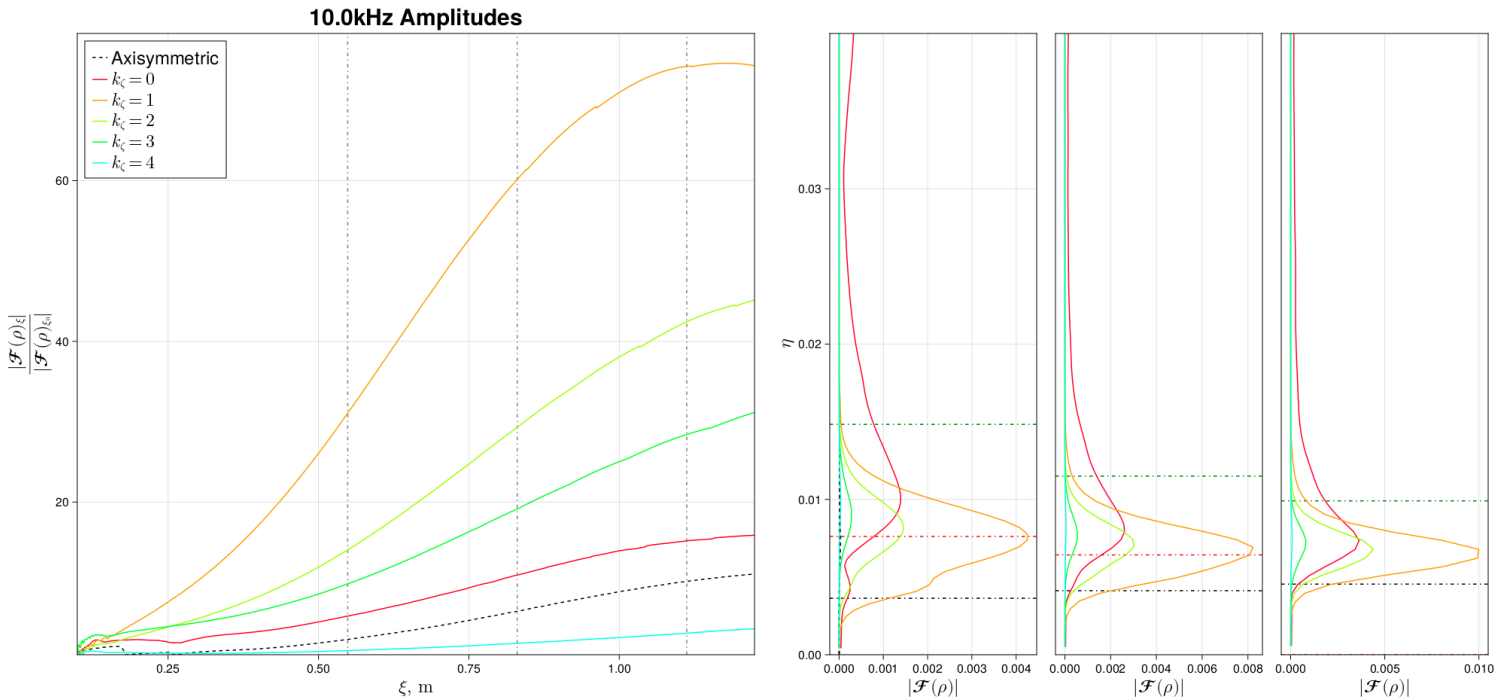

Spatial evolution and wallnormal profiles of the axisymmetric and spanwise 10kHz modes.

Shape of Density Disturbances

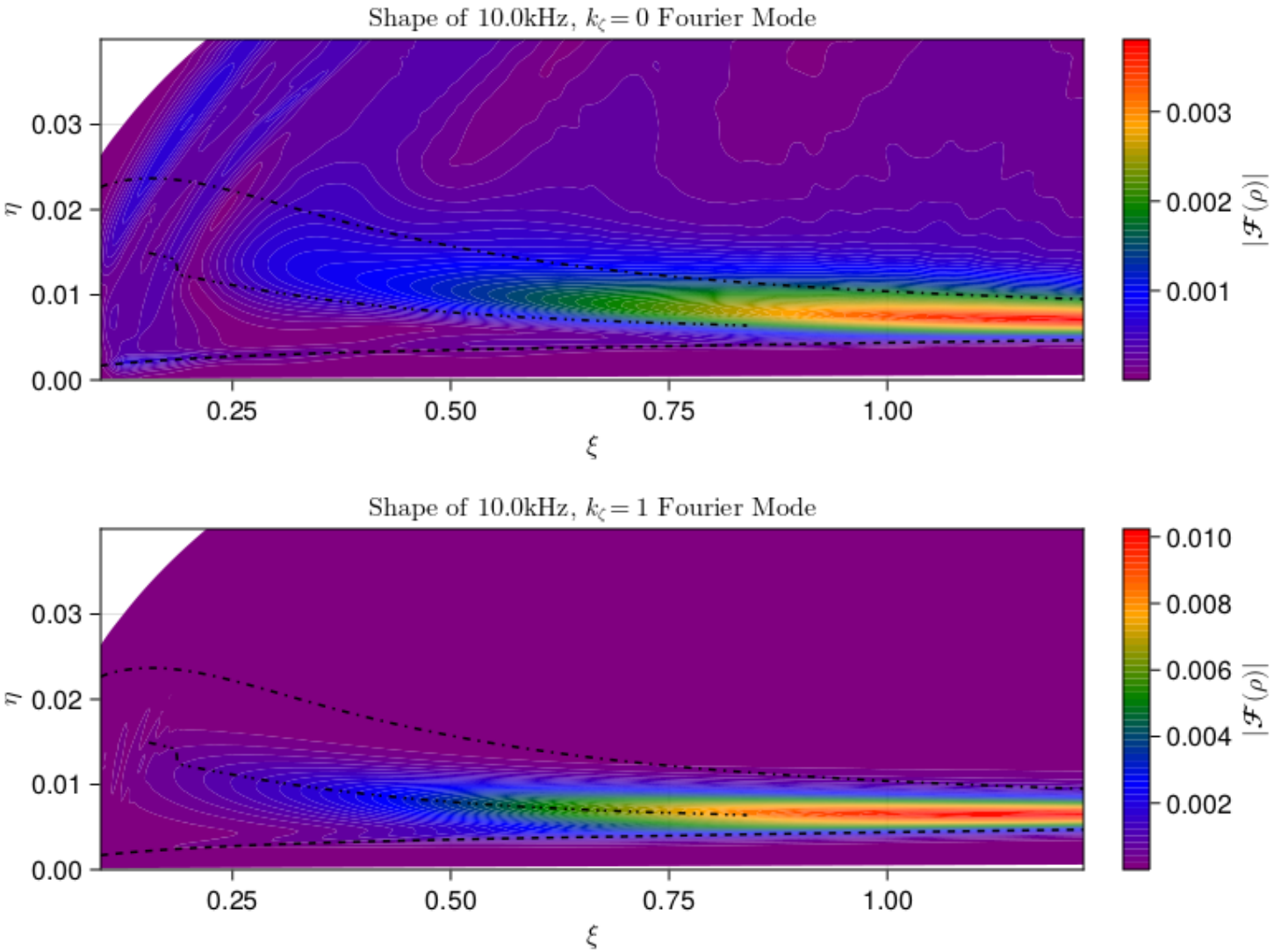

Shape of the axisymmetric and first spanwise density modes.

What Have we Learned?

- Axisymmetric simulations do not accurately capture axisymmetric modes.

What Have we Learned?

- Axisymmetric simulations do not accurately capture axisymmetric modes.
- Inflectional instability is more unstable to three dimensional modes, in contrast to linear analyses.